Supplementary information

Wintertime aerosol chemistry and haze evolution in an extremely polluted city of Northern China: Insights from highly time-resolved real-time measurements

Haiyan Li[1,2], Qi Zhang[2], Qiang Zhang[3,4], Chunrong Chen[3], Litao Wang[5], Zhe Wei[5], Shan Zhou[2], Caroline Parworth[2], Bo Zheng[1], Francesco Canonaco[6], André S. H. Prévôt[6], Ping Chen[7], Hongliang Zhang[7], Kebin He[1,4,8]

[1] State Key Joint Laboratory of Environment Simulation and Pollution Control, School of Environment, Tsinghua University, Beijing 100084, China

[2] Department of Environmental Toxicology, University of California, Davis, CA 95616, USA

[3] Ministry of Education Key Laboratory for Earth System Modeling, Center for Earth System Science, Tsinghua University, Beijing 100084, China

[4] Collaborative Innovation Center for Regional Environmental Quality, Beijing 100084, China

[5] Department of Environmental Engineering, Hebei University of Engineering, Handan, Hebei 056038, China

[6] Laboratory of Atmospheric Chemistry, Paul Scherrer Institute, 5232 PSI Villigen, Switzerland

[7] Handix LLC, Boulder, CO 8031, USA

[8] State Environmental Protection Key Laboratory of Sources and Control of Air Pollution Complex, Tsinghua University, Beijing 100084, China

Corresponding Author: Qiang Zhang (qiangzhang@tsinghua.edu.cn), Kebin He (hekb@tsinghua.edu.cn)

Text S1. Analysis to determine the best solution for ME-2

Using the multi-linear engine (ME-2) implemented with the toolkit SoFi (Source Finder), organic source apportionment was performed with the so-called a value approach. The a value determines the extent to which the resolved factor profiles ($f_{j,solution}$) or time series ($g_{i,solution}$) are allowed to vary from the input ones (fj, gi) (Canonaco et al., 2013):

$f_{j,solution} = f_j \pm a \cdot f_j$,

$g_{i,solution} = g_i \pm a \cdot g_i$,

To separate an individual HOA factor in addition to CCOA, BBOA and OOA, we only constrained the mass spectra of HOA in this study, using the reference profile from Ng et al. (2011). Some important criterions to select the optimal solution with a value varying from 0 to 1 are shown in Fig. S2-S6. Generally, increasing a value decreases Q and the ratio of Q to Q_{exp}, due to additional degrees of freedom. However, the size of the change of Q/Qexp over different a values is not significant (Fig. S2a). In addition, the explained variation (EV) could indicate how much variation in each variable is explained by each factor. According to Paatero (2004), a variable should be considered only if the unexplained EV for that variable is less than 25% (Fig. S2c).

Combining the analysis of factor profiles and time series of each factor across different a values, there is no significant variations for CCOA and OOA. By contrast, with different constraint levels, large changes were found for HOA and BBOA, which were mixed during PMF analysis. As shown in Fig. S3a, moving from a constrained run to a less constrained situation apportioned more signals to larger m/z for HOA profile. For a values from 0.2 to 1.0, fractions of m/z smaller than 50 for BBOA profile were significantly enhanced and the time series of BBOA were similar to those of OOA. These results indicated that solutions for a value of 0 and 0.1 were more reasonable. This was further evidenced by the diurnal profiles of each factor and their correlations with external tracers over different a values. To allow some degrees of freedom for model run, we chose the results for a value of 0.1 to be the best solution in this study.

47 **Table S1.** Summary of online measurements (μg/m^3) using an Aerodyne ACSM or AMS during wintertime in China.

Sampling site	Handan, Hebei	Beijing	Beijing	Beijing	Beijing	Lanzhou, Gansu	Nanjing, Jiangsu	Jiaxing, Zhejiang	Ziyang, Sichuan
Location	36.57°N, 114.50°E	39.99°N, 116.31°E	39.97°N, 116.37°E	39.97°N, 116.37°E	39.97°N, 116.37°E	36.05°N, 103.85°E,	32.05°N, 118.77°E	30.8°N, 120.8°E	30.15°N, 104.64°E
Period	Dec.3,2015-Feb.5, 2016	Nov.22-Dec.22, 2010	Nov.21,2011-Jan.20,2012	Jan.1-Feb.1,2013	Dec.17,2013-Jan.17,2014	Jan.10-Feb.4,2014	Dec.1-31, 2013	Dec.11-23, 2010	Dec.3,2012-Jan.5,2013
instrument	ACSM[a]	HR-AMS[b]	ACSM	HR-AMS	HR-AMS	HR-AMS	ACSM	HR-AMS	HR-AMS
NR-PM_1	173.4	63.5	66.2	89.2	63.9	53.6	90.2	34.9	52.9
Sulfate	28.1	8.7	9.3	19.6	9.6	7.2	14.3	7.1	12.2
Nitrate	26.1	6.8	10.6	12.5	7	9.5	22.3	7.5	8.9
Ammonium	21.4	7.7	8.6	8.9	5.1	5.9	12.5	4.9	8.2
Chloride	16.6	5.8	3.3	3.6	3.8	1.7	2.7	2.7	2.1
Organic	81.2	34.5	34.4	44.6	38.4	29.3	38.4	12.7	21.5
HOA	6	4.7	5.8	4.9	3.8	2.6	5	5	3.2
COA	N.D.[c]	6.7	6.5	8.9	6.9	5.8	5	N.D.	N.D.
BBOA	20.7	4.1	N.D.	N.D.	3.3	3.2	5.8	3.8	3

CCOA	23.1	8.2	11.4	6.7	7.6	5.3	N.D.	N.D.	N.D.
OOA	31.4	N.D.	10.7	N.D.	16.9	N.D.	N.D.	3.8	N.D.
SV-OOA	N.D.	N.D.	N.D.	11.6	N.D.	7	N.D.	N.D.	7.8
LV-OOA	N.D.	N.D.	N.D.	12.5	N.D.	5.6	8.8	N.D.	7.5
LO-OOA	N.D.	4.3	N.D.	N.D.	N.D.	N.D.	4.6	N.D.	N.D.
MO-OOA	N.D.	6.2	N.D.	N.D.	N.D.	N.D.	9.2	N.D.	N.D.
Reference	this study	Hu et al. (2016a)	Sun et al. (2013)	Zhang et al. (2014)	Sun et al. (2016)	Xu et al. (2016)	Zhang et al. (2015)	Huang et al. (2012)	Hu et al. (2016b)

[a] Aerosol Chemical Speciation Monitor (ACSM)

[b] High Resolution Time-of-Flight Aerosol Mass Spectrometer (HR-AMS)

[c] N.D. = not detected.

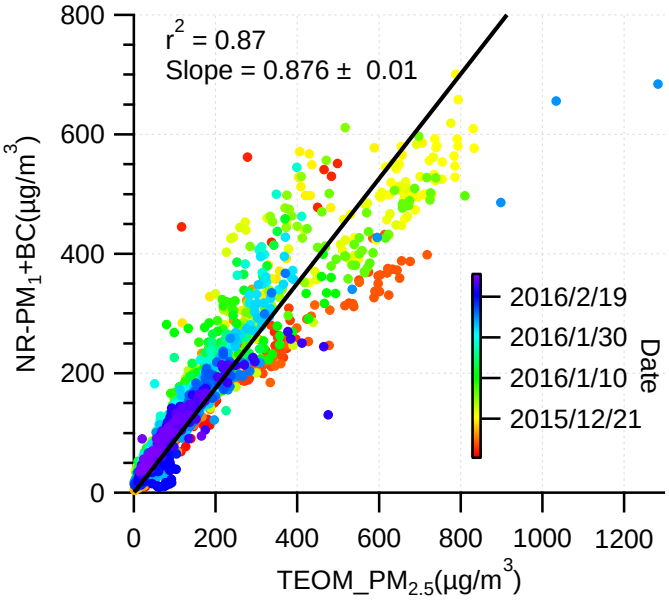

Figure S1. Correlation of NR-PM_1 measured by ACSM plus BC measured by MAAP with $PM_{2.5}$ measured by TEOM.

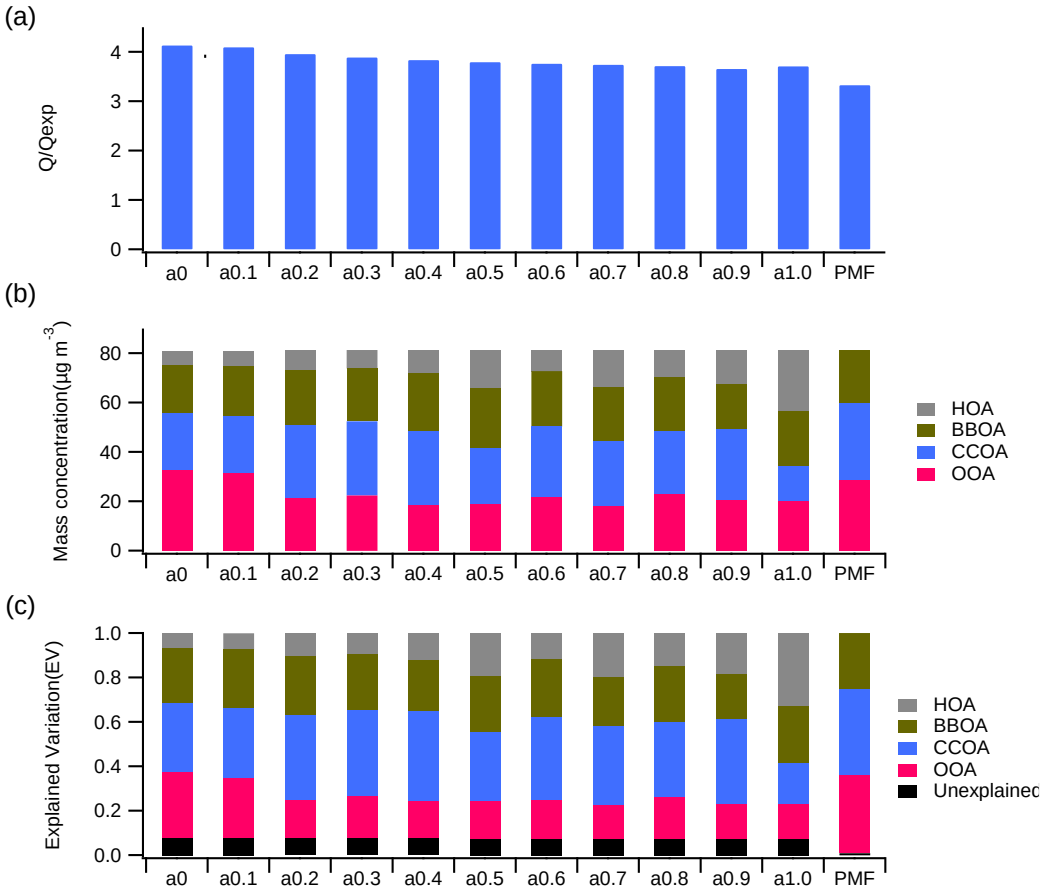

Figure S2. (a) Values of Q/Qexp, (b) mass concentrations of each factor and (c) explained variation (EV) for each factor and total unexplained variation (UEV) for different model runs. The PMF result shown here is for 3-factor solution.

(a)

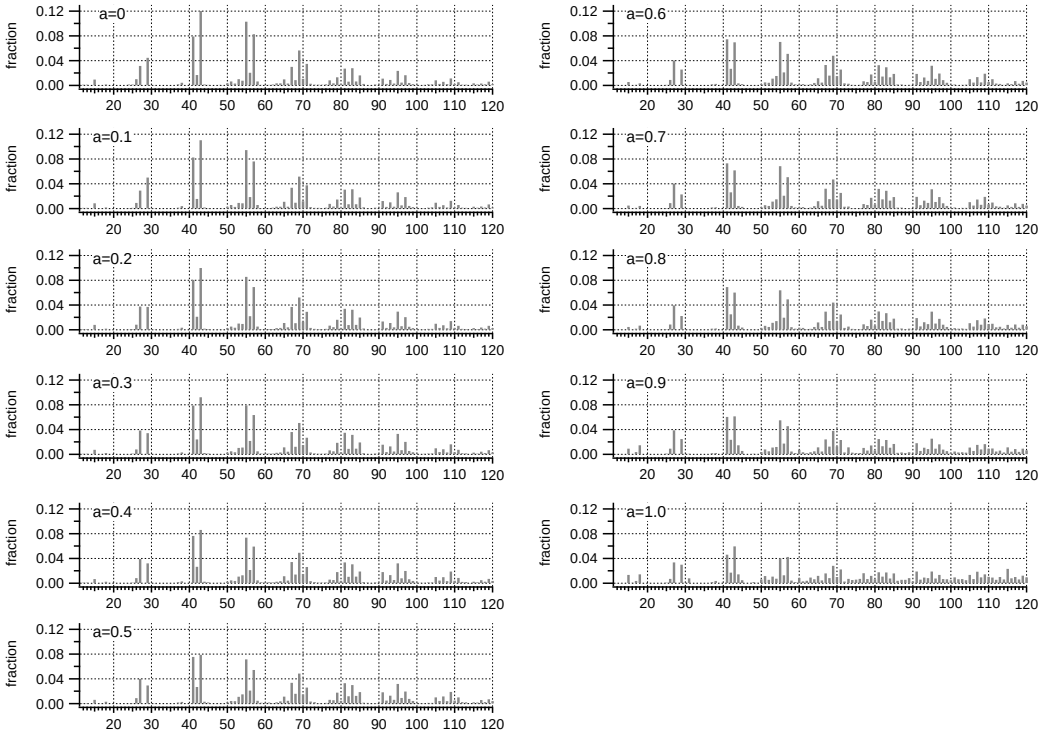
a=0
a=0.1
a=0.2
a=0.3
a=0.4
a=0.5
a=0.6
a=0.7
a=0.8
a=0.9
a=1.0
fraction
0.12
0.08
0.04
0.00
20 30 40 50 60 70 80 90 100 110 120

61

62

(b)

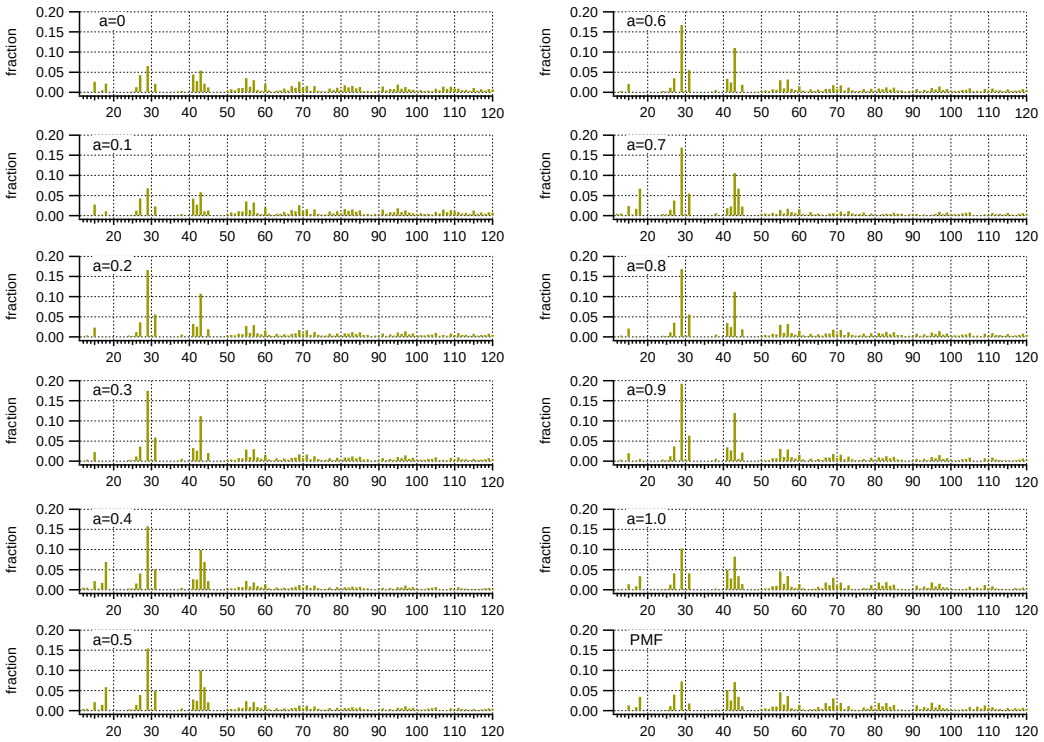
a=0
a=0.1
a=0.2
a=0.3
a=0.4
a=0.5
a=0.6
a=0.7
a=0.8
a=0.9
a=1.0
PMF
fraction
0.20
0.15
0.10
0.05
0.00
20 30 40 50 60 70 80 90 100 110 120

63

64

(c)

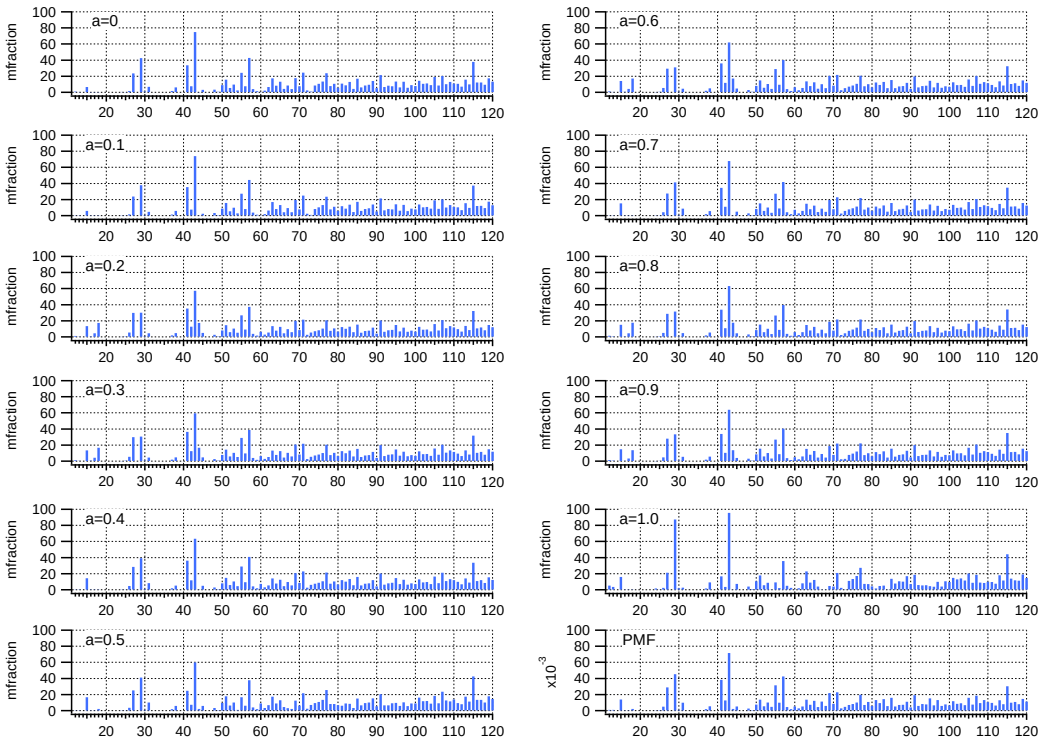
a=0
a=0.1
a=0.2
a=0.3
a=0.4
a=0.5
a=0.6
a=0.7
a=0.8
a=0.9
a=1.0
PMF
mfraction
x10-3
0
20
40
60
80
100
20
30
40
50
60
70
80
90
100
110
120

65

66

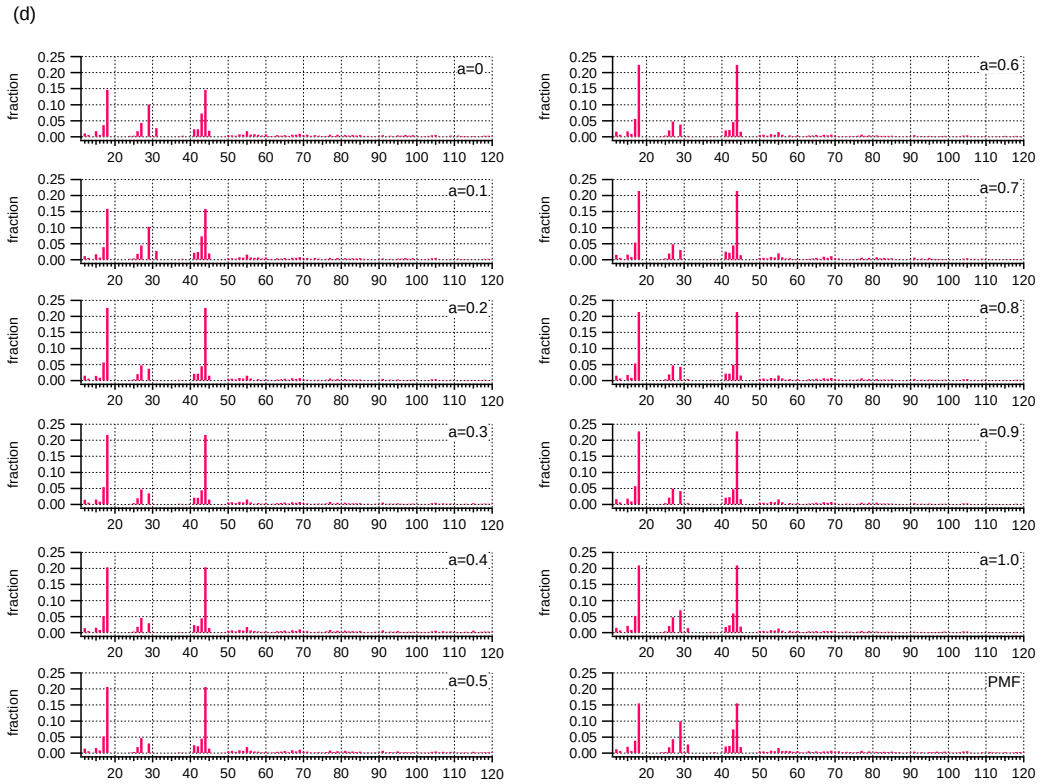

Figure S3. Factor profiles of (a) HOA, (b) BBOA, (c) CCOA and (d) OOA for different model runs

(a)

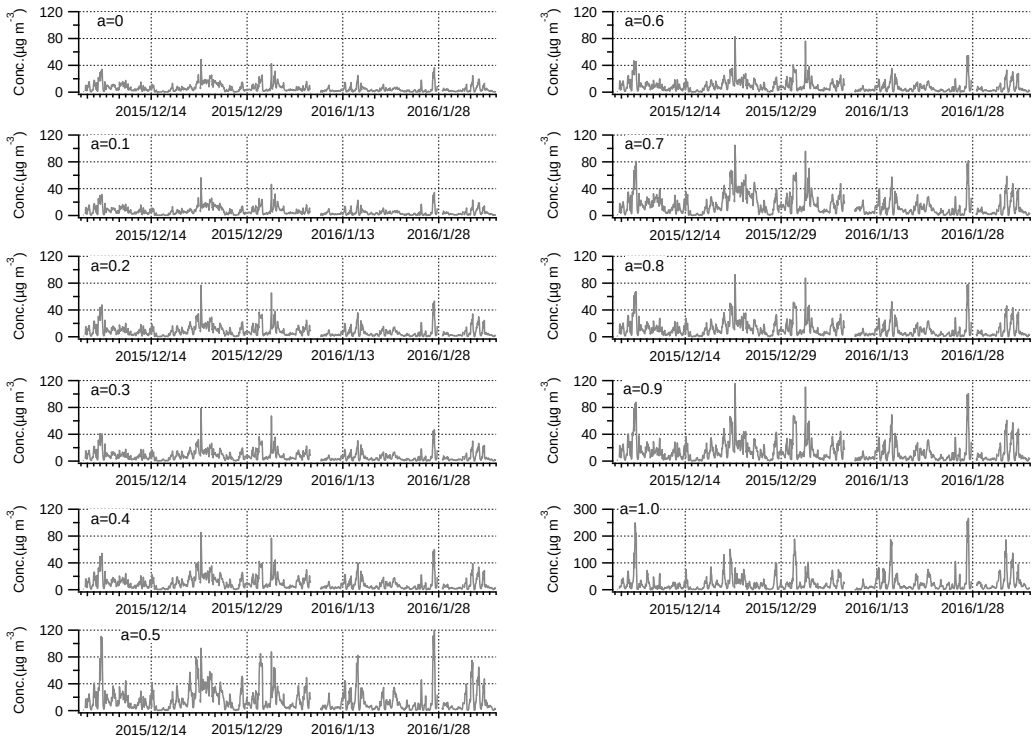
a=0
a=0.1
a=0.2
a=0.3
a=0.4
a=0.5
a=0.6
a=0.7
a=0.8
a=0.9
a=1.0
Conc.(μg m-3)
2015/12/14
2015/12/29
2016/1/13
2016/1/28

70

71

(b)

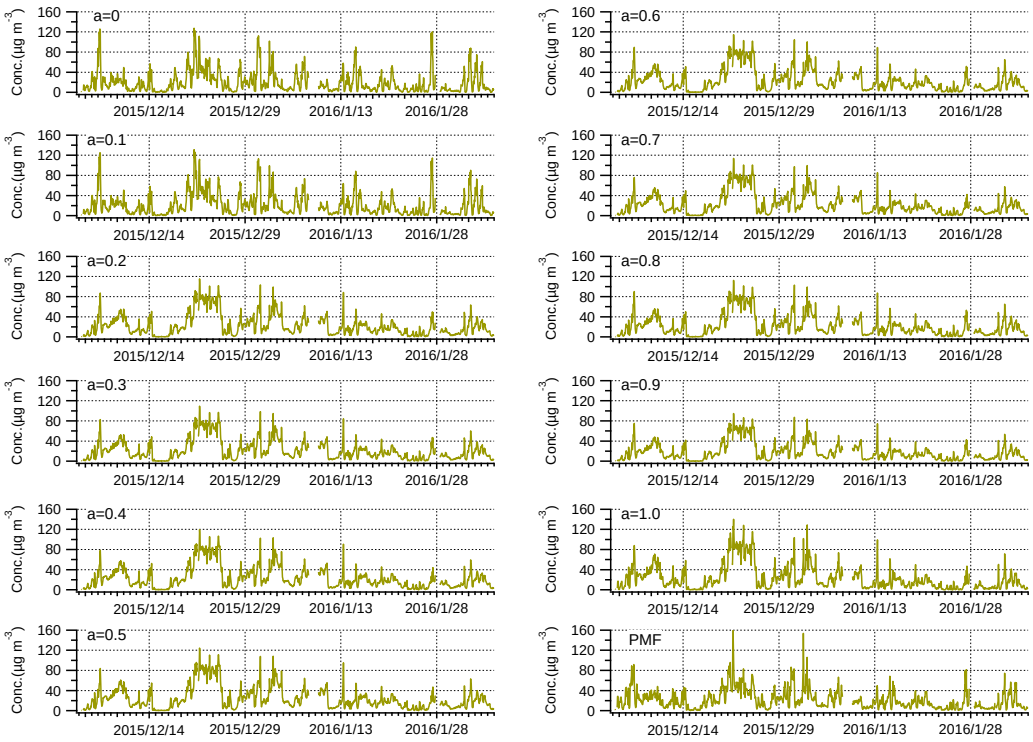
a=0
a=0.1
a=0.2
a=0.3
a=0.4
a=0.5
a=0.6
a=0.7
a=0.8
a=0.9
a=1.0
PMF
Conc.(μg m-3)
0
40
80
120
160
2015/12/14
2015/12/29
2016/1/13
2016/1/28

72

73

(c)

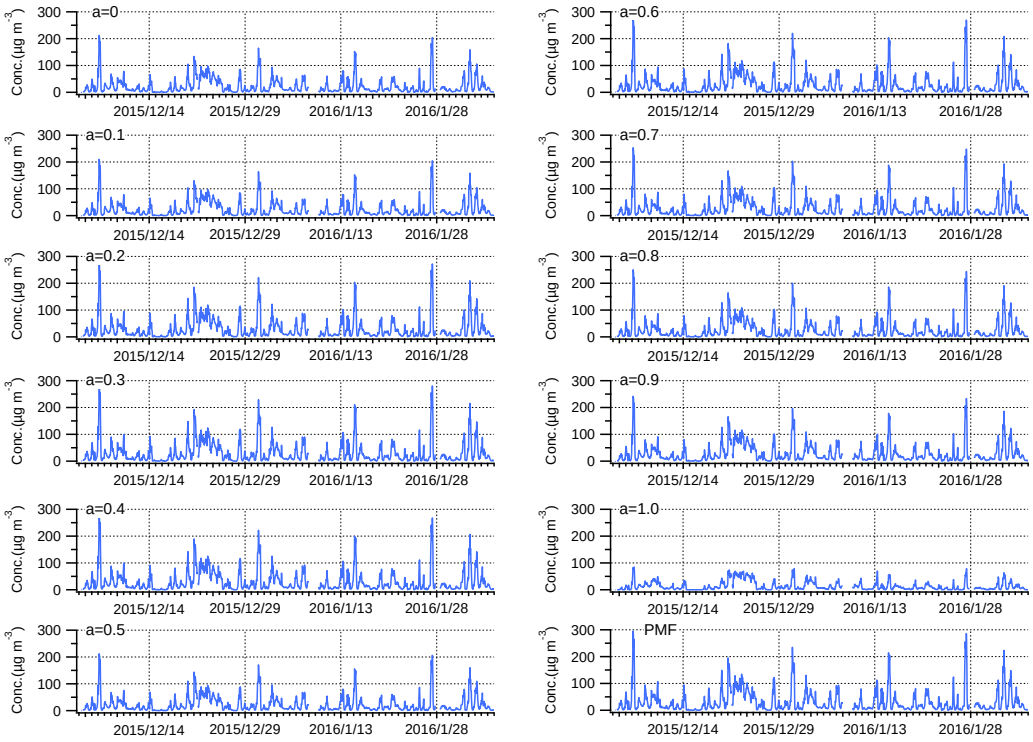
a=0
a=0.1
a=0.2
a=0.3
a=0.4
a=0.5
a=0.6
a=0.7
a=0.8
a=0.9
a=1.0
PMF
Conc.(μg m-3)
300
200
100
0
2015/12/14
2015/12/29
2016/1/13
2016/1/28

74

75

(d)

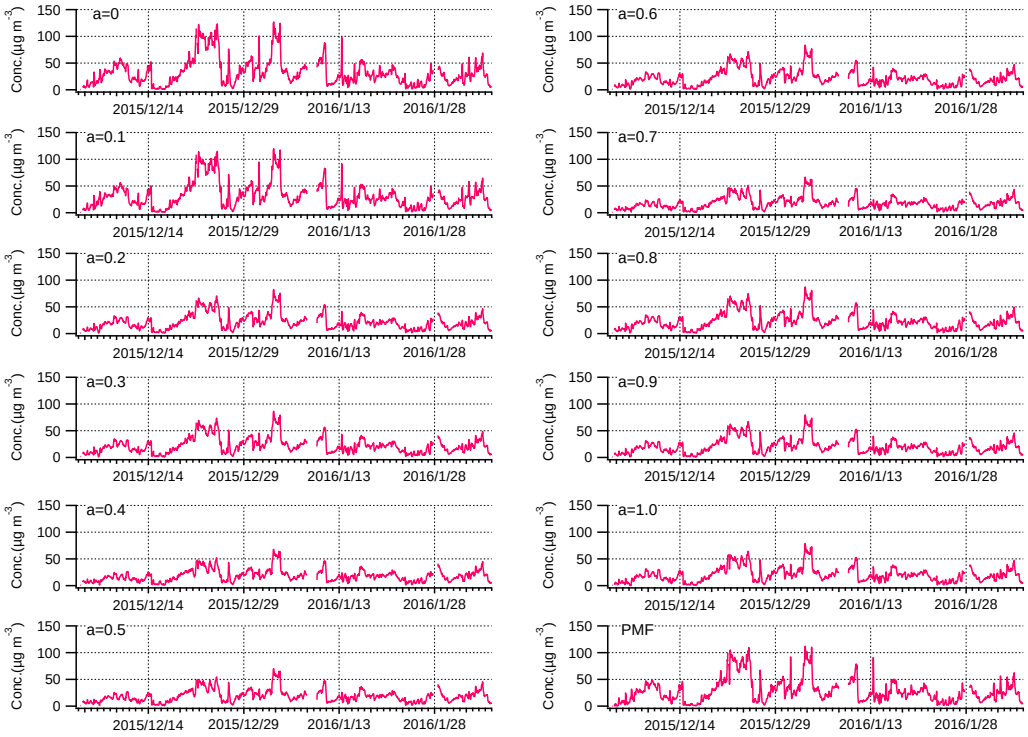

Figure S4. Time series of (a) HOA, (b) BBOA, (c) CCOA and (d) OOA for different model runs.

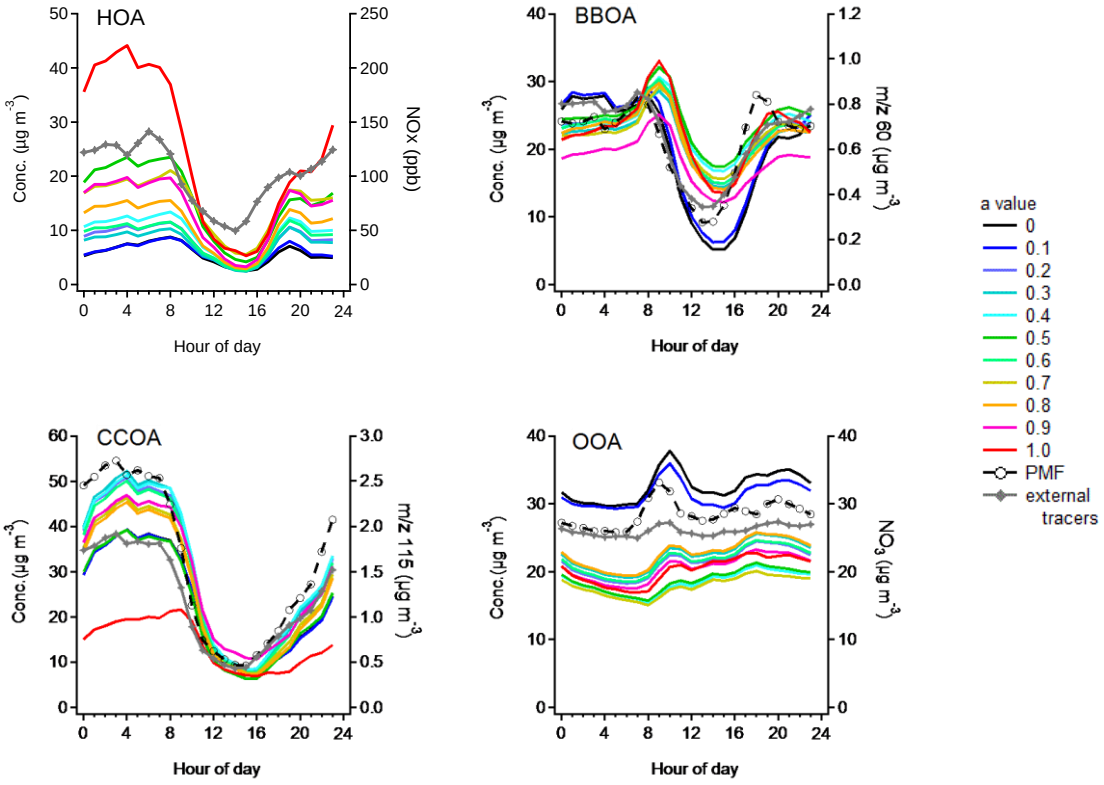

79

80 **Figure S5.** Mean diurnal variations of HOA, BBOA, CCOA and OOA for different model runs, with the
81 variations of their external tracers on the right axis.

82

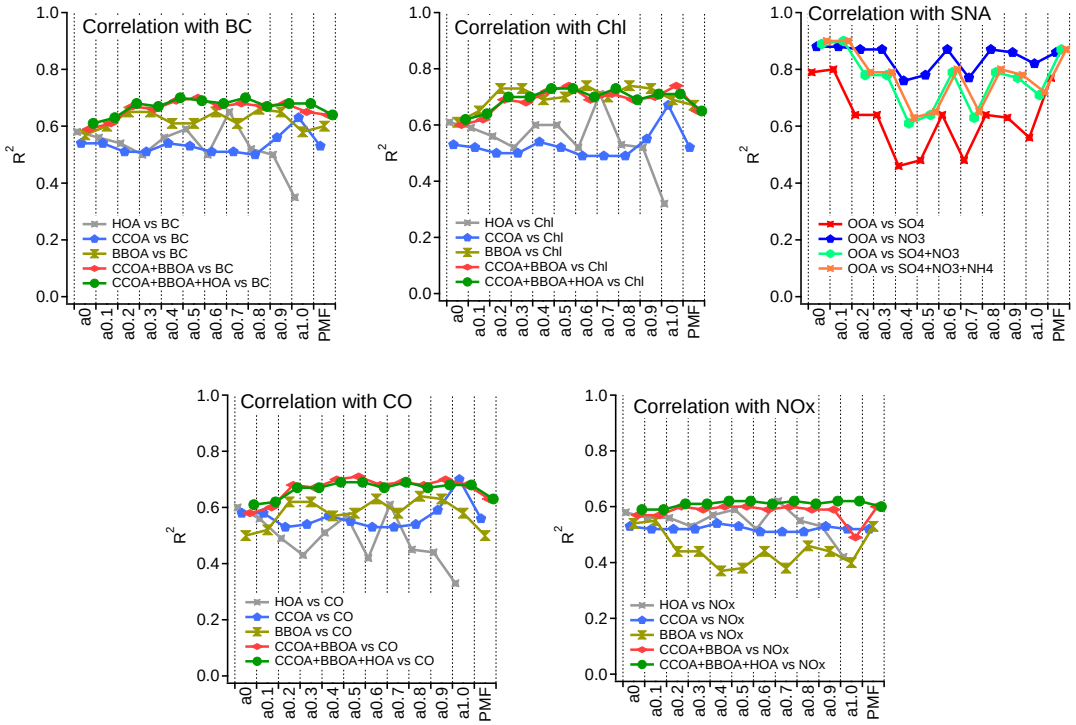

Figure S6. Correlations R^2 (Pearson) between the time series of OA factors and the time series of external tracers as a function of model runs.

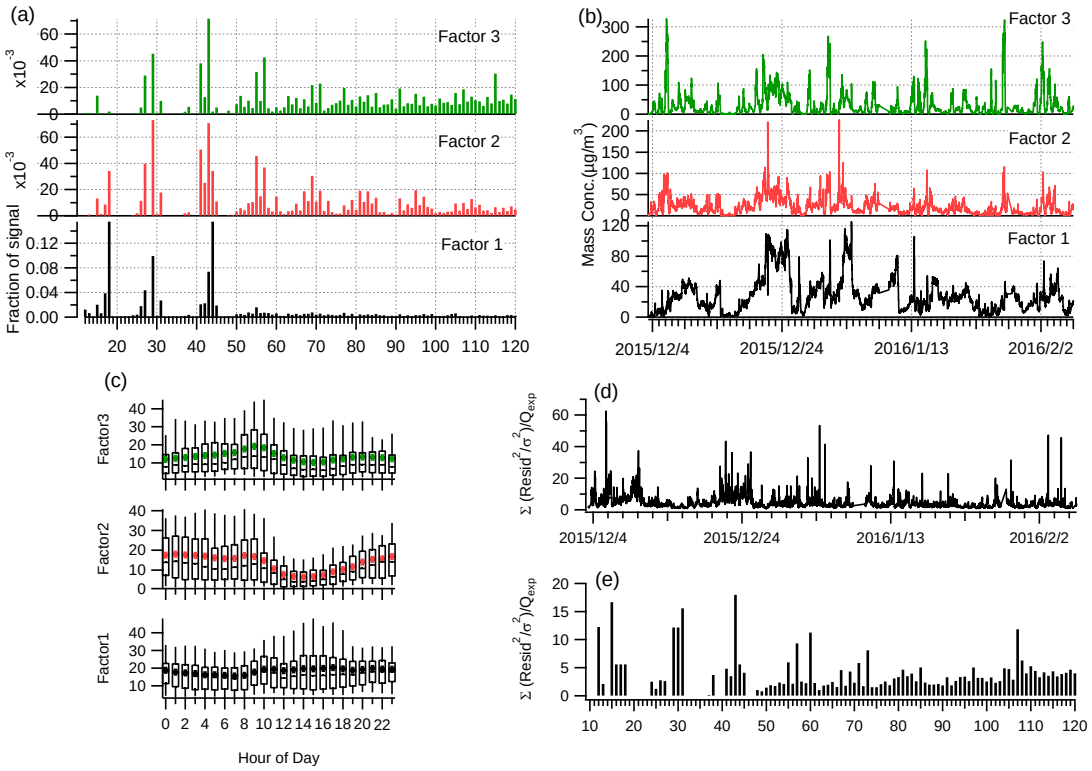

Figure S7. (a) Spectral profiles, (b) time series, (c) diurnal patterns, (d) time series of Q/Qexp, and (e) spectral profile of Q/Qexp for 3-factor solution of PMF analysis.

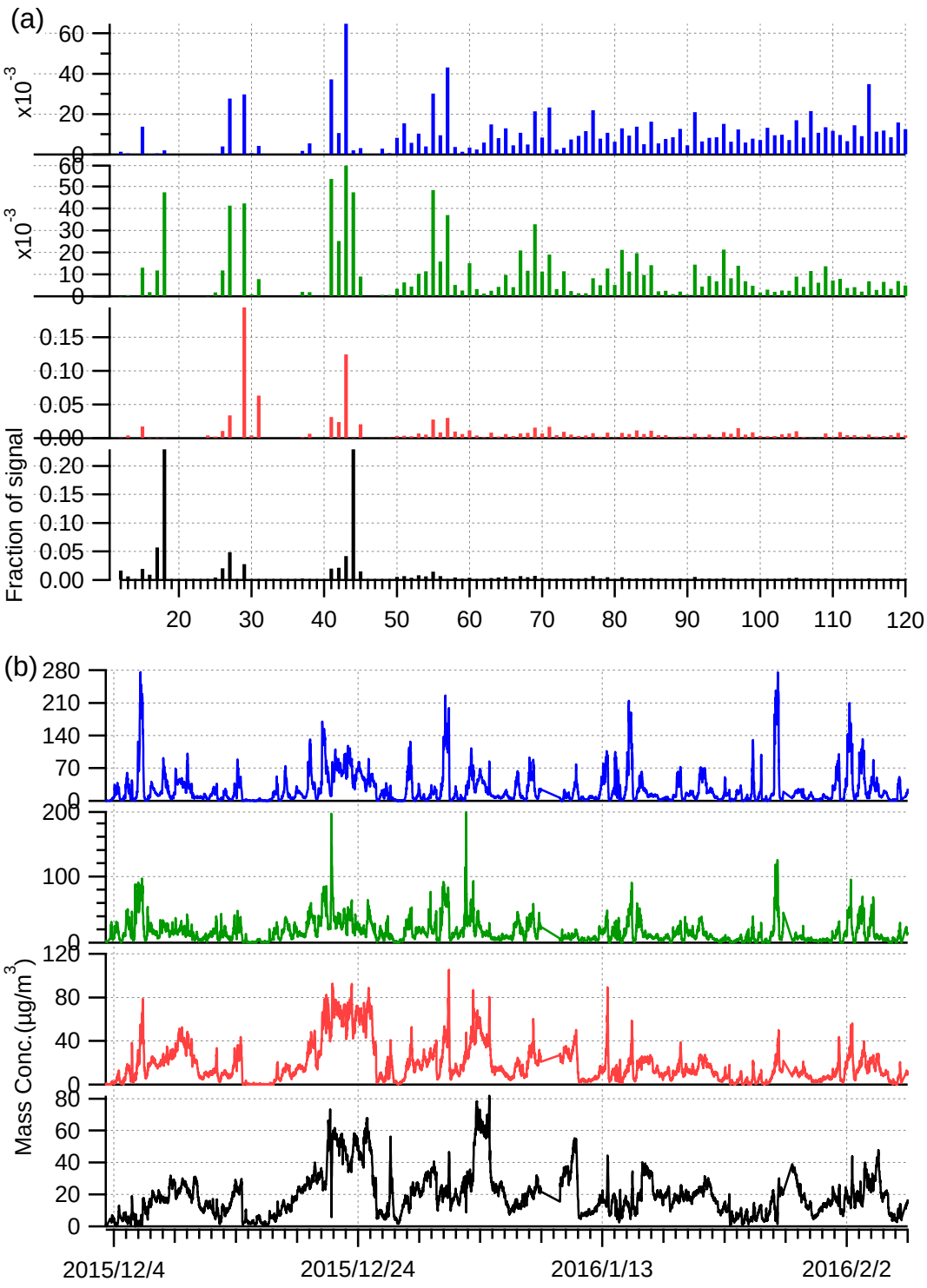

Figure S8. (a) Spectral profiles and (b) time series for 4-factor solution of PMF analysis.

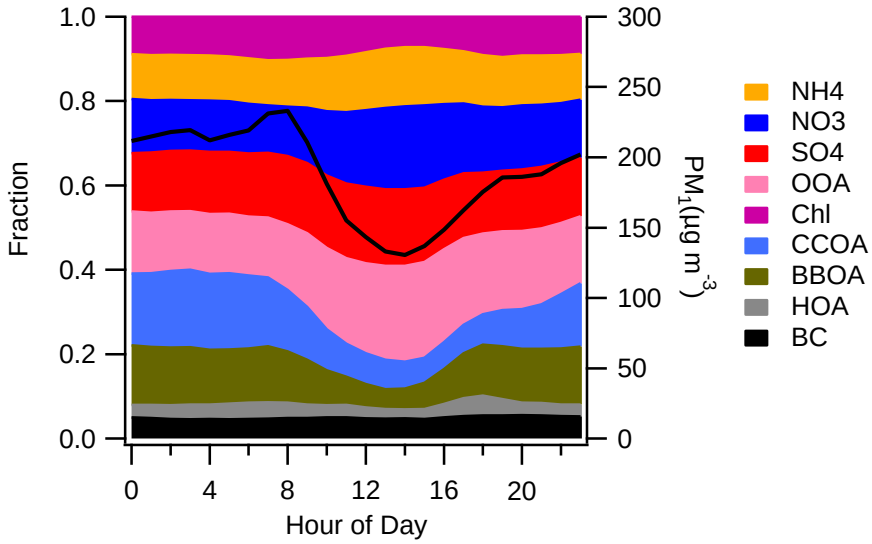

94

95 **Figure S9.** Average diurnal cycles of the mass fractions of aerosol species.

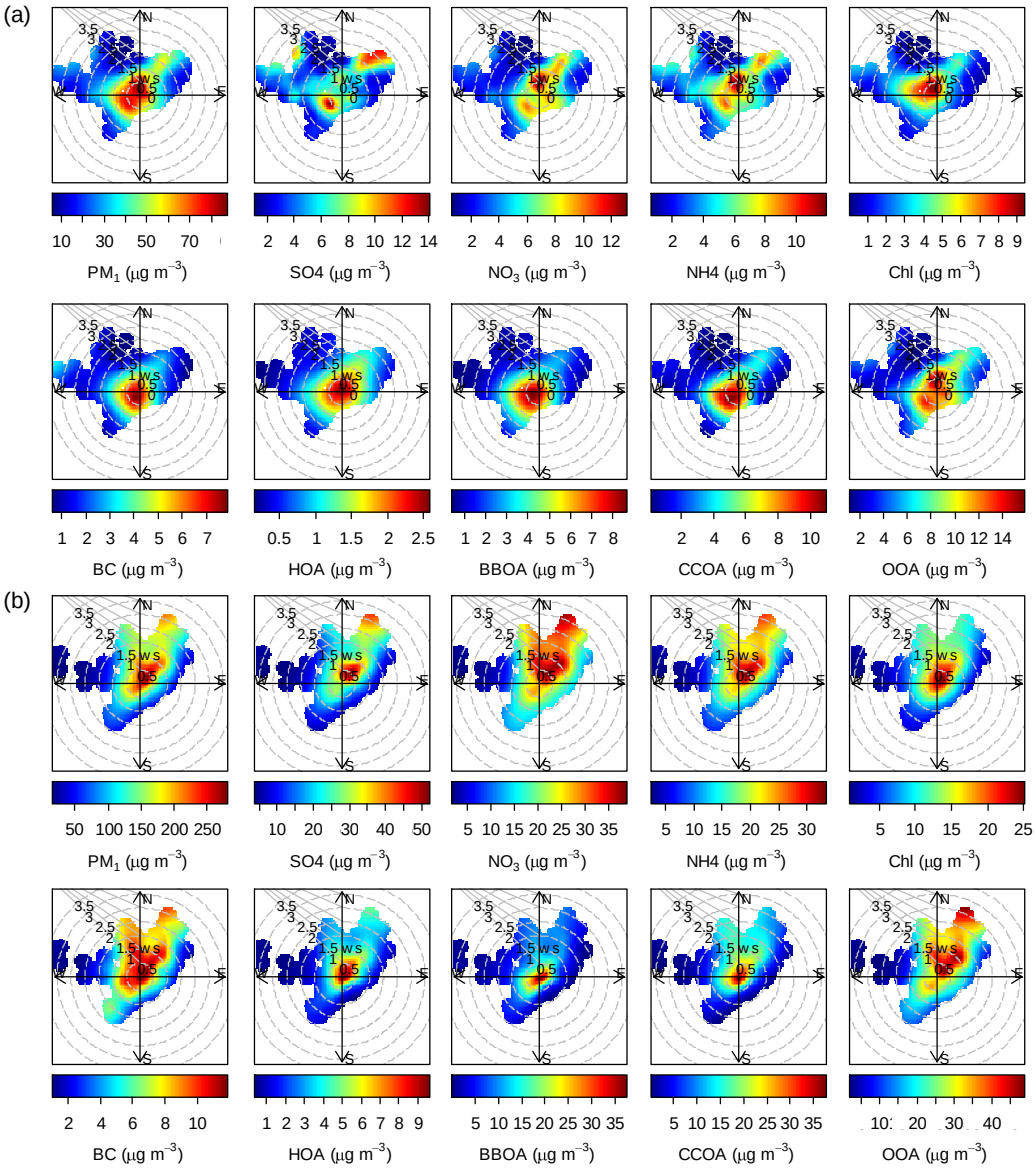

Figure S10. Polar plots of aerosol components as a function of wind speed and wind direction for (a) non-polluted and (b) polluted periods.

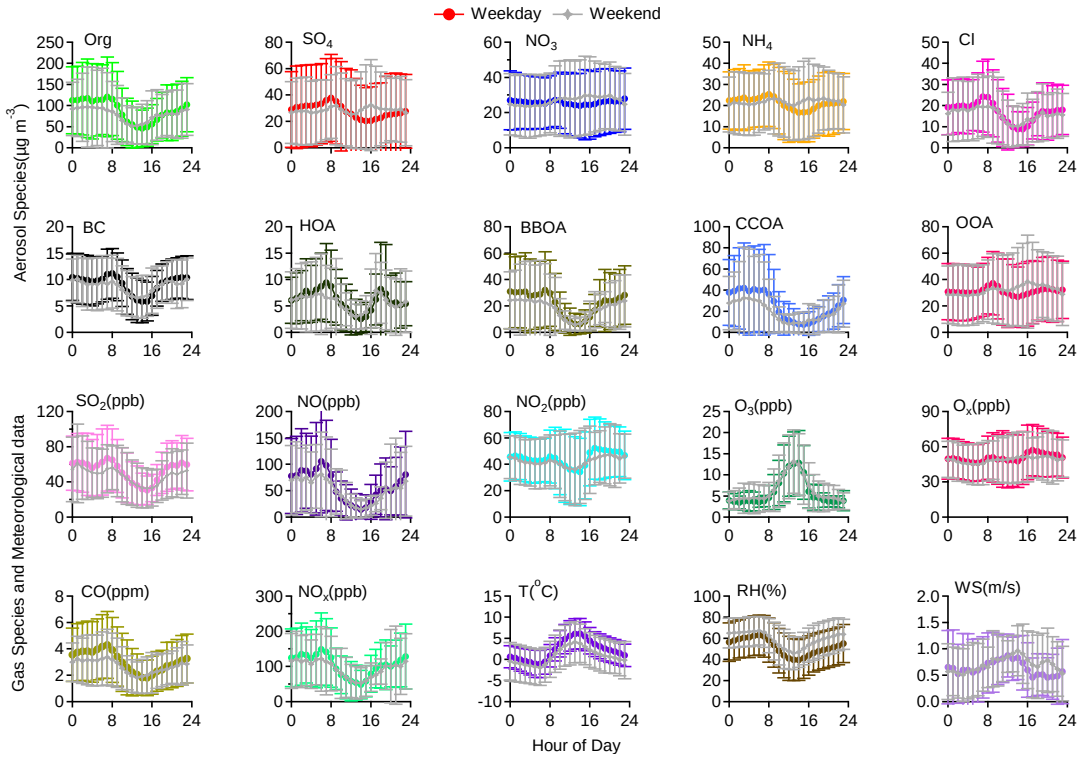

Figure S11. Average diurnal profiles along with the standard deviation of PM_1 species, four OA factors identified from PMF analysis, various gas-phase species, and meteorological parameters for weekdays (Monday to Friday inclusive) and weekends (Saturday and Sunday) during the campaign.

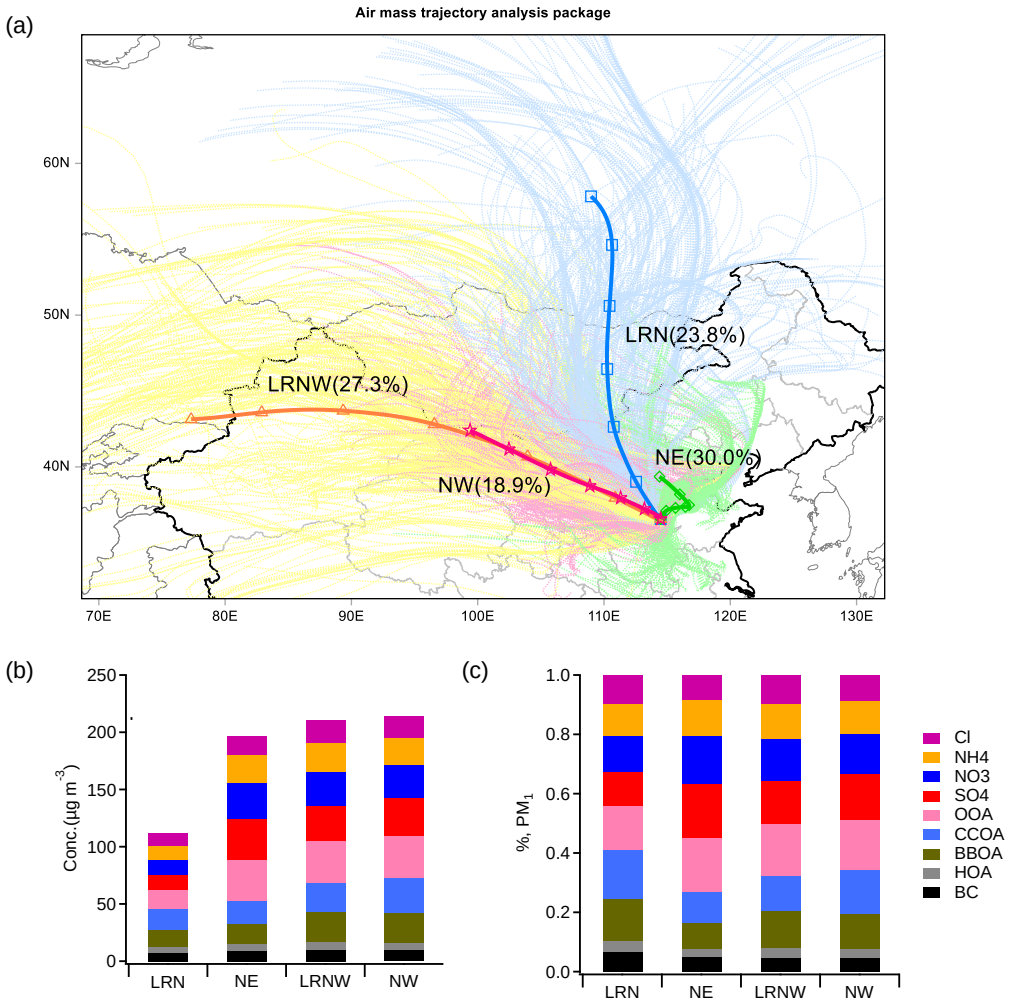

Figure S12. (a) Back trajectories of air masses arriving at Handan every hour for 500 m above ground level and four clusters determined using the inbuilt function of HYSPLIT for the entire campaign. The four clusters represent air masses long-range transported from the north (LRN, 23.8%), from the northeast (NE, 30.0%), from the northwest (NW, 18.9%), and long-range transported from the northwest (LRNW, 27.3%). (b) Mass concentrations and (c) mass fractions of aerosol species for each cluster.

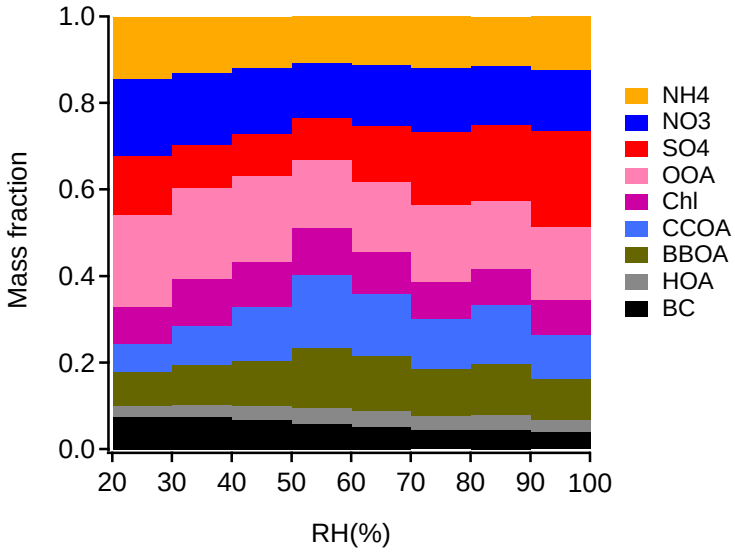

Figure S13. The RH-binned bulk composition of submicron aerosols.

References

Hu, W., Hu, M., Hu, W., Jimenez, J. L., Yuan, B., Chen, W., Wang, M., Wu, Y., Chen, C., Wang, Z., Peng, J., Zeng, L., and Shao, M.: Chemical composition, sources and aging process of submicron aerosols in Beijing: contrast between summer and winter, J. Geophys. Res., 121, 1955–1977, doi:10.1002/2015JD024020, 2016a.

Hu, W., Hu, M., Hu, W.-W., Niu, H., Zheng, J., Wu, Y., Chen, W., Chen, C., Li, L., Shao, M., Xie, S., and Zhang, Y.: Characterization of submicron aerosols influenced by biomass burning at a site in the Sichuan Basin, southwestern China, Atmos. Chem. Phys., 16, 13213-13230, doi:10.5194/acp-16-13213-2016, 2016b.

Huang, X. F., Xue, L., Tian, X. D., Shao, W. W., Sun, T. L., Gong, Z. H., Ju, W. W., Jiang, B., Hu, M., and He, L. Y.: Highly time-resolved carbonaceous aerosol characterization in Yangtze River Delta of China: Composition, mixing state and secondary formation, Atmos. Environ., 64, 200–207, doi:10.1016/j.atmosenv.2012.09.059, 2013.

Ng, N. L., Canagaratna, M. R., Jimenez, J. L., Zhang, Q., Ulbrich, I. M., and Worsnop, D. R.: Real-time methods for estimating organic component mass concentrations from aerosol mass spectrometer data, Environ. Sci. Technol., 45, 910–916, 2011.

Paatero, P.: User's guide for positive matrix factorization programs PMF2 and PMF3, 2004.

Sun, Y. L., Wang, Z. F., Fu, P. Q., Yang, T., Jiang, Q., Dong, H. B., Li, J., and Jia, J. J.: Aerosol composition, sources and processes during wintertime in Beijing, China, Atmos. Chem. Phys., 13, 4577-4592, doi:10.5194/acp-13-4577-2013, 2013.

Sun, Y., Du, W., Fu, P., Wang, Q., Li, J., Ge, X., Zhang, Q., Zhu, C., Ren, L., Xu, W., Zhao, J., Han, T., Worsnop, D. R., and Wang, Z.: Primary and secondary aerosols in Beijing in winter: sources, variations and processes, Atmos. Chem. Phys., 16, 8309-8329, doi:10.5194/acp-16-8309-2016, 2016.

Xu, J., Shi, J., Zhang, Q., Ge, X., Canonaco, F., Prévôt, A. S. H., Vonwiller, M., Szidat, S., Ge, J., Ma, J., An, Y., Kang, S., and Qin, D.: Wintertime organic and inorganic aerosols in Lanzhou, China: Sources, processes and comparison with the results during summer, Atmos. Chem. Phys. Discuss., doi:10.5194/acp-2016-278, in review, 2016.

Zhang, J. K., Sun, Y., Liu, Z. R., Ji, D. S., Hu, B., Liu, Q., and Wang, Y. S.: Characterization of submicron aerosols during a month of serious pollution in Beijing, 2013, Atmos. Chem. Phys., 14, 2887-2903, doi:10.5194/acp-14-2887-2014, 2014.

Zhang, Y. J., Tang, L., Yu, H., Wang, Z., Sun, Y., Qin, W., Chen, W., Chen, C., Ding, A., Wu, J., Ge, S., Chen, C., and Zhou, H.-C.: Chemical composition, sources and evolution processes of aerosol at an urban site in Yangtze River Delta, China during wintertime, Atmos. Environ., 123, 339–349, doi:10.1016/j.atmosenv.2015.08.017, 2015.